View metadata, citation and similar papers at core.ac.uk

brought to you by CORE

provided by University of Queensland eSpace

Calculation of product state distributions from resonance decay via Lanczos subspace filter diagonalization: Application to HO 2

Hong Zhang and Sean C. Smith

Citation: The Journal of Chemical Physics **115**, 5751 (2001); doi: 10.1063/1.1400785

View online: http://dx.doi.org/10.1063/1.1400785

View Table of Contents: http://scitation.aip.org/content/aip/journal/jcp/115/13?ver=pdfcov

Published by the AIP Publishing

Articles you may be interested in

A complex guided spectral transform Lanczos method for studying quantum resonance states
J. Chem. Phys. **141**, 244114 (2014); 10.1063/1.4905083

Unimolecular rovibrational bound and resonance states for large angular momentum: J = 20 calculations for H O 2
J. Chem. Phys. **123**, 014308 (2005); 10.1063/1.1949609

Computing resonance energies, widths, and wave functions using a Lanczos method in real arithmetic
J. Chem. Phys. **122**, 244107 (2005); 10.1063/1.1942494

Comparison of Chebyshev, Faber, and Lanczos propagation-based methods for calculating resonances
J. Chem. Phys. **112**, 5263 (2000); 10.1063/1.481096

The unimolecular dissociation of HCO. IV. Variational calculation of Siegert states
J. Chem. Phys. **110**, 9887 (1999); 10.1063/1.478862

Reuse of AIP Publishing content is subject to the terms: https://publishing.aip.org/authors/rights-and-permissions. Downloaded to IP: 130.102.82.69 On: Fri, 07 Oct 2016 05:32:49

Calculation of product state distributions from resonance decay via Lanczos subspace filter diagonalization: Application to HO_2

Hong Zhang and Sean C. Smith[a)]
Department of Chemistry, School of Molecular and Microbial Sciences, The University of Queensland, Qld 4072, Brisbane, Australia

(Received 23 March 2001; accepted 17 July 2001)

Resonance phenomena associated with the unimolecular dissociation of HO_2 have been investigated quantum-mechanically by the Lanczos homogeneous filter diagonalization (LHFD) method. The calculated resonance energies, rates (widths), and product state distributions are compared to results from an autocorrelation function-based filter diagonalization (ACFFD) method. For calculating resonance wave functions via ACFFD, an analytical expression for the expansion coefficients of the modified Chebyshev polynomials is introduced. Both dissociation rates and product state distributions of O_2 show strong fluctuations, indicating the dissociation of HO_2 is essentially irregular. © *2001 American Institute of Physics.* [DOI: 10.1063/1.1400785]

I. INTRODUCTION

The study of unimolecular dissociation reactions is fundamentally important to many areas of pure and applied chemistry.[1,2] When a molecule fragments, we are commonly interested in answers to the following two questions: at what rate did the reaction occur, and afterwards, in what quantum states are the products?

There are several distinct methods for estimating the rate constants of unimolecular reactions. These include statistical theories, classical trajectory simulations, and quantum theories.[3–6] The rigorous quantum-mechanical way to describe unimolecular reaction rates is to compute Siegert states[7] (resonance states), which are quasibound, so-called compound states that are embedded in the continuum. These are eigenfunctions of the Schrödinger equation with outgoing wave boundary conditions. Because of the complex boundary conditions, the eigenvalues are necessarily complex, $\{E_R - i\Gamma/2\}$. The real part of the eigenvalue, E_R, is the energy of the metastable state of the molecule, while its unimolecular decay rate, k, is given in terms of the imaginary part, $\Gamma/\hbar$. (The latter relationship is only true if the resonance states are nonoverlapping.[8]) Unlike bound states, resonance states have a finite width in the energy domain and their wave functions extend to infinity. Since they are scattering states, resonances are generally more complicated to calculate than bound states.

The energy of a resonance is essentially determined by the potential energy surface (PES) in its inner region, while its width depends on the coupling between the inner region and the exit channel. The product state distributions reflect scattering from resonance to product states through a transitional state, and thus contain additional clues about the intra- and intermolecular dynamics of the system. Each resonance has a unique width and is associated with unique product state distributions. In order to fully understand the unimolecular dissociation dynamics, therefore, it is useful to consider all three observables for as many resonances as possible.

Quantum-mechanically, resonances can be treated in either the time-independent or time-dependent domain. In the former, one has to solve the homogeneous time-independent Schrödinger equation

$$(E - \hat{H}')\Psi_E = 0. \tag{1}$$

Here, $\hat{H}' = \hat{H} - i\hat{V}_{\text{abs}}$, i.e., a complex absorbing potential augments the Hamiltonian ($\hat{H}$) to invoke the appropriate boundary conditions at ''infinite'' product separation, and Ψ_E is the resonance wave function. In practice, Eq. (1) is challenging to solve for reactions involving polyatomic molecules, and several methods incorporating the variational principle[5,9] and filter diagonalization[10–16] have been developed to tackle large systems. While arguably the most successful, filter diagonalization (FD) approaches suffer storage problems when performed in a large primary representation (e.g., a multidimensional DVR or finite basis). To overcome the memory bottleneck, Yu and Smith introduced quasiminimum residual (QMR) and minimum residual (MINRES) filter diagonalization,[17–20] which typically requires three complex vectors to be stored. A key feature of Yu and Smith's QMRFD and MINRESFD approaches is that the entire calculation is carried out within a Lanczos subspace. Consequently, a single Lanczos subspace is sufficient for analyzing the entire spectrum, since representing the Hamiltonian tridiagonally makes it a straightforward exercise to generate a new set of filtered states in the next energy window by solving QMR equations implicitly within the subspace. Recently, for the calculation of bound and resonance states, we have developed an improved algorithm[21] (the Lanczos homogeneous filter diagonalization algorithm, LHFD) which more efficiently generates filtered states within a Lanczos subspace by solving homogeneous linear systems with a simple recursion formula. It is partly the aim of this paper to extend the algorithm for computing product state distributions (PSDs).

a)Electronic mail: s.smith@chemistry.uq.edu.au

 © 2001 American Institute of Physics

Reuse of AIP Publishing content is subject to the terms: https://publishing.aip.org/authors/rights-and-permissions. Downloaded to IP: 130.102.82.69 On: Fri, 07 Oct 2016 05:32:49

In time-dependent approaches, on the other hand, one must propagate an initial wave packet according to the time-dependent Schrödinger equation to generate correlation functions, $C(t)$. These functions reflect the motion of the wave packet and are therefore a convenient means to visualize the molecular dynamics. In principle, one can obtain resonances by directly analyzing correlation functions (via a half-Fourier transform).[22,23] However, to get a high-resolution spectrum, one must propagate a wave packet for a long time. To avoid expensive long-time propagations, Neuhauser *et al.*[12] proposed an autocorrelation function-based filter diagonalization (ACFFD) scheme to calculate resonances. An attractive feature of this scheme is its low storage demands—eigenvalues in different energy windows can be obtained from a single sequence of autocorrelation functions without the need to explicitly construct the filtered states. Mandelshtam *et al.*[14] combined this scheme with a modified real Chebyshev propagation approach,[13,24,25] and implemented a discrete box-like FD formalism. In this paper, both time-independent LHFD and time-dependent ACFFD methods shall be compared using a model triatomic system: the hydroperoxyl radical, HO_2.

The HO_2 system has been extensively studied due to its importance in combustion and atmospheric chemistry. The ground state PES of HO_2 has a very deep well supporting over 350 bound states of odd parity, and therefore has a relatively high density of states, making this system very complicated and a challenging one to characterize. Several groups have performed both bound- and resonances calculations on this system. For example, Mandelshtam *et al.*[13] have successfully computed bound- and resonance state energies by employing FD based on a damped Chebyshev recursion in a primary representation. Kendrick and Pack[26,27] obtained consistent resonance energies and widths using the coupled channel method. Zhang *et al.*[28,29] have calculated both bound- and resonance energies by employing Fourier transform of the time-autocorrelation functions. Schinke *et al.*[5,30] investigated this system using a modification of the log-derivative version of Kohn's variational principle, and compared the quantum rate constants with that of statistical RRKM theories.

This article is organized as follows. We describe the LHFD method in Sec. II alongside the ACFFD method to be used later for comparison. In Sec. III shall give the results of the three-dimensional calculations performed on the unimolecular HO_2 dissociation reaction. Section IV concludes.

II. THEORETICAL METHODS

A. Lanczos homogeneous filter diagonalization (LHFD) method

1. Resonance energies and widths

In the LHFD method[21] we first project the augmented Hamiltonian into a Krylov subspace using the Lanczos method.[31] Inside the subspace, the Hamiltonian (represented as a tridiagonal matrix, T_M) can be used to perform FD calculations for various energy windows. Most FD approaches require the solution of inhomogeneous systems of linear equations $(H-EI)x=b$ (I is the identity matrix and E the filtering energy) to converge filtered states. In contrast, our LHFD method, as its name suggests, relies upon solving $(H-E)x=0$. If the filtering energy E is a true eigenvalue, then in exact algebra the result of the homogeneous recursion is to generate the corresponding eigenvector (unnormalized). However, if E is not an eigenvalue then the same recursion plays the role of an extremely efficient filtering operation.[21] The advantage associated with this choice is that the linear system can be solved effectively by a simple three-term recursion. Additionally, matrix-vector multiplications involving the tridiagonal Hamiltonian require merely three-dot products.

In more detail, the LHFD algorithm for characterizing resonances can be summarized as follows:

(i) Choose a normalized, randomly generated initial vector $v_1 \neq 0$ and set $\beta_1 v_0 = 0$. Then, use the three-term Lanczos algorithm for complex-symmetric matrices[32]

$$\beta_{k+1} v_{k+1} = \hat{H}' v_k - \alpha_k v_k - \beta_k v_{k-1}, \tag{2}$$

to project the non-Hermitian augmented Hamiltonian into a Krylov subspace. The $M \times M$ tridiagonal representation of the Hamiltonian, T_M, has diagonal elements $\alpha_k = (v_k|\hat{H}|v_k)$ and subdiagonal elements $\beta_k = (v_{k-1}|\hat{H}|v_k)$. Note that a complex-symmetric inner product is used (i.e., bra vectors are not complex conjugated).

(ii) For all $j = 1,2,...,j_{\max}$, generate filtered states $\phi(E_j)$ by solving the homogeneous linear system

$$(E_j - T_M)|\phi(E_j)\rangle = 0. \tag{3}$$

Here, a backward substitution recursion is employed:

(a) Choose ϕ_M, the Mth element of $\phi(E_j)$, to be arbitrary (but nonzero; usually set $\phi_M = 1$), and calculate

$$\phi_{M-1} = \frac{1}{\beta_M}(E_j \phi_M - \alpha_M \phi_M). \tag{4}$$

(b) For $k = M-1, M-2, ..., 2$, update scalar ϕ_{k-1}:

$$\beta_k \phi_{k-1} = E_j \phi_k - \alpha_k \phi_k - \beta_{k+1} \phi_{k+1}. \tag{5}$$

(iii) Construct the overlap matrix with elements $S_{jj'} = (\phi(E_j)|\phi(E_{j'}))$ and subspace Hamiltonian matrix with elements $W_{jj'} = (\phi(E_j)|T_M|\phi(E_{j'}))$. Note that $W_{jj'}$ can be calculated using a three-term summation

$$W_{jj'} = \sum_{k=1}^{M} [\phi_k(E_j)\beta_k \phi_{k-1}(E_{j'}) + \phi_k(E_j)\alpha_k \phi_k(E_{j'}) + \phi_k(E_j)\beta_{k+1}\phi_{k+1}(E_{j'})]. \tag{6}$$

(iv) Solve the generalized complex-symmetric eigenvalue problem $WB = SB\varepsilon$ to obtain the complex energies, $\{\varepsilon\}$.

(v) Span the energy domain by repeating (ii)–(iv) window by window.

Due to the tridiagonal structure of the subspace Hamiltonian, one can generate *all* the elements of a filtered state by specifying practically any value for the scalar ϕ_M. Since the choice is arbitrary, the solution must be normalized after step (ii) to yield the true filtered state, $\phi(E_j) \leftarrow \eta_j \times \phi(E_j)$. To check the convergence of the eigenvalues as well as the qual-

Reuse of AIP Publishing content is subject to the terms: https://publishing.aip.org/authors/rights-and-permissions. Downloaded to IP: 130.102.82.69 On: Fri, 07 Oct 2016 05:32:49

ity of the eigenpairs generated by the above iterative methods, one can typically compute the error norm about the eigenenergy E,

$$\sigma(E)=\|(T_M-E)\zeta(E)\|, \tag{7}$$

where the Lanczos eigenvector $\zeta(E)$ is cheaply regenerated for each complex eigenenergy using Eq. (3). Clearly, true eigenvalues should have small error norms and can thus be distinguished from any unconverged/spurious eigenvalues.

2. Product state distributions

The complex resonance wave functions in Eq. (1) obey the Siegert-type boundary conditions asymptotically, i.e., they are products of outgoing radial waves in the scattering coordinate, R say, and internal eigenfunctions in the remaining coordinates. For our target system HO_2, the resonance wave function in terms of Jacobi coordinates (R,r,θ) is written

$$\Psi_{E_R}(R_\infty,r,\theta)=\sum_n a_n(E_R)\sqrt{\frac{\mu_{H,O_2}}{\hbar k_n}}e^{ik_nR_\infty}\varphi_n(r,\theta), \tag{8}$$

where

$$a_n(E_R)=\sqrt{\frac{\hbar k_n}{\mu_{H,O_2}}}e^{-ik_nR_\infty}\langle\varphi_n(r,\theta)|\Psi_{E_R}(R_\infty,r,\theta)\rangle, \tag{9}$$

and $n=(\nu,j)$, and $k_n=\sqrt{2\mu_{H,O_2}\hbar^{-2}(E_R-\varepsilon_n)}$.

Within the subspace, we can use Eq. (8) to perform the asymptotic scattering analysis. The product rotational state distribution, $P_n=|a_n(E_R)|^2$, may be acquired by computing

$$P_n=\frac{\hbar k_n}{\mu_{H,O_2}}|\langle\varphi_n(r,\theta)|\Psi_{E_R}(R_\infty,r,\theta)\rangle|^2. \tag{10}$$

The analysis is done in the region where the interaction potential is small, but before the region where the absorbing potential is nonzero (where the resonance wave function is exponentially decreasing).

One can transform wave functions between the primary representation and the Lanczos subspace through

$$\zeta(E_R)=V^T\Psi_{E_R}, \tag{11}$$

$$\Psi_{E_R}=V\zeta(E_R)=\sum_{i=1}^{M}\zeta_i(E_R)v_i, \tag{12}$$

where $V=[v_1,v_2,\ldots,v_M]$ is the column-orthonormal Lanczos vector matrix. So, using Eq. (12), the inner product appearing in Eq. (10) can be re-expressed

$$\begin{aligned}\langle\varphi_n(r,\theta)|\Psi_{E_R}(R_\infty,r,\theta)\rangle&=\sum_{i=1}^{M}\zeta_i(E_R)\langle\varphi_n(r,\theta)|v_i(R_\infty,r,\theta)\rangle\\&=\sum_{i=1}^{M}\zeta_i(E_R)\chi_i^{(n)}.\end{aligned} \tag{13}$$

The vectors $\chi^{(n)}=V^T\varphi_n$ are the subspace projections of the internal eigenfunctions. Thus, from a single set of Lanczos iterations, one can calculate the energies *and* the product state distributions for different resonances.

B. Autocorrelation function-based filter diagonalization (ACFFD) method

1. Resonance energies and widths

In this FD scheme, the most important and computationally demanding step is to calculate time-correlation functions, $C(t)$. To acquire them, we employ the modified Chebyshev polynomial algorithm proposed by Mandelshtam and Taylor *et al.*[13,24,25] and described as follows. Incorporating a real-valued damping function, $\hat{\gamma}$, time-correlation functions can be expressed (with $\hbar=1$) as

$$\begin{aligned}C_n=(\Phi_0,\Phi(n\tau))&=\left(\Phi_0,\sum_{k=0}^{k_{\max}}a_k(n\tau)\xi_k^{\hat{\gamma}}\right)\\&=\sum_{k=0}^{k_{\max}}a_k(n\tau)(\Phi_0,\xi_k^{\hat{\gamma}})\\&=\sum_{k=0}^{k_{\max}}a_k(n\tau)c_k,\end{aligned} \tag{14}$$

where

$$a_k(n\tau)=(2-\delta_{k0})e^{-i\bar{H}n\tau}(-i)^kJ_k(\Delta Hn\tau). \tag{15}$$

In the above equations, $\bar{H}=0.5(H_{\max}+H_{\min})$, $\Delta H=0.5(H_{\max}-H_{\min})$, $H_{\min}(H_{\max})$ is the smallest (largest) eigenvalue of the Hamiltonian, J_k is a Bessel function, Φ_0 is the initial wave packet (a randomly generated real vector), and τ is the size of the time propagation step. The number of Chebyshev expansion terms needed for convergence can be estimated typically as[33] $k_{\max}(n\tau)\cong\Delta Hn\tau+20$, which is increased as the propagation time becomes longer. The main task is the calculation of real correlation functions $\{c_k\}$, which can be realized by a modified Chebyshev recursion

$$\xi_{k+1}^{\hat{\gamma}}=e^{-\hat{\gamma}}(2\hat{H}_{\text{norm}}\xi_k^{\hat{\gamma}}-e^{-\hat{\gamma}}\xi_{k-1}^{\hat{\gamma}}), \tag{16}$$

with $\xi_0^{\hat{\gamma}}=\Phi_0$, $\xi_1^{\hat{\gamma}}=e^{-\hat{\gamma}}\hat{H}_{\text{norm}}\xi_0^{\hat{\gamma}}$, and $\hat{H}_{\text{norm}}=(\hat{H}-\bar{H})/\Delta H$. This propagation method is a large step propagation, and is different from standard complex Chebyshev step-by-step propagation. The advantage associated with this algorithm is that for the heaviest part of the computation, namely the calculation of the real scalars $\{c_k\}$, a real algorithm can be employed.

By choosing each filtered state as a partial Fourier transform of the time-dependent wave function $\Phi(t)$ and employing the evolution operator $\hat{U}=e^{-i\tau\hat{H}}$, one can set up a small-sized generalized eigenproblem

$$U^{(1)}B=U^{(0)}B\varepsilon. \tag{17}$$

The diagonal elements of the matrices $U^{(p)}(p=0,1)$ are written

$$U_{jj}^{(p)}=\sum_{l=0}^{2M}(M-|M-l|+1)C_{l+p}z_j^{-l} \tag{18}$$

while the off-diagonal elements are

Reuse of AIP Publishing content is subject to the terms: https://publishing.aip.org/authors/rights-and-permissions. Downloaded to IP: 130.102.82.69 On: Fri, 07 Oct 2016 05:32:49

$$U_{jj'}^{(p)}=\frac{1}{z_j-z_{j'}}\Bigg[z_j\sum_{l=0}^{M}C_{l+p}z_{j'}^{-l}-z_{j'}\sum_{l=0}^{M}C_{l+p}z_j^{-l}-\frac{1}{z_j^M}\sum_{l=M+1}^{2M}C_{l+p}z_{j'}^{M-l+1}+\frac{1}{z_{j'}^M}\sum_{l=M+1}^{2M}C_{l+p}z_j^{M-l+1}\Bigg], \tag{19}$$

where $z_j=e^{-iE_j\tau}$, and M takes the value of $(n_{\max}-2)/2$ with $n_{\max}\tau$ being the largest propagation time. The eigenvalues of $\hat{U}$ are $u_k=e^{-i\tau E_k}$, i.e., $E_k=i\ln u_k/\tau$. After generating discrete autocorrelation functions, we store this vector, then perform FD calculations for arbitrarily chosen windows using the same vector.

2. Product state distributions

Resonance wave function can be calculated through a partial time–energy Fourier transformation of the time-dependent wave packet

$$\Psi(E)=\int_0^\infty dt\,\exp(iEt)\Phi(t). \tag{20}$$

Using a damped Chebyshev expansion for $\Phi(t)$, namely Eq. (14), we can derive an analytical expression for the expansion coefficients of $\Psi(E)$ through a partial Fourier transform of the complex time-dependent Chebyshev expansion coefficients $\{a_k(t)\}$. First, we rewrite the wave function

$$\Psi(E)=\sum_{k=0}\hat{\xi_k^\gamma}\int_0^\infty dt\,\exp(iEt)a_k(t)=\sum_{k=0}\hat{\xi_k^\gamma}d_k(E), \tag{21}$$

where

$$d_k(E)=(2-\delta_{k0})(-i)^k\int_0^\infty dt\,\exp[i(E-\bar{H})t]J_m(\Delta Ht). \tag{22}$$

Then, for $H_{\min}<E<H_{\max}$, we can use an appropriate integral formula[34] to simplify Eq. (22)

$$d_k(E)=(2-\delta_{k0})(-i)^k\frac{\exp\left[-ik\arcsin\left(\frac{\bar{H}-E}{\Delta H}\right)\right]}{\sqrt{(\Delta H)^2-(\bar{H}-E)^2}}. \tag{23}$$

In form, the above expression for the expansion coefficient, $d_k(E)$, is different from the ones given by Neuhauser *et al.*,[33] Mandelshtam *et al.*,[35] and Kouri *et al.*[36] This has prompted us to check its validity by comparing it numerically with the other three. We have found it to give similar results to the formulas of Neuhauser *et al.* and Mandelshtam *et al.*, but quite different results from the formula of Kouri *et al.*

Like the time-independent LHFD method, we can arrive at an expression for product state distributions after obtaining the resonance wave functions

$$P_n=|a_n(E_R)|^2=\frac{\hbar k_n}{\mu_{\mathrm{H,O_2}}}\left|\sum_{k=0}d_k(E_R)\omega_k^{(n)}\right|^2, \tag{24}$$

with

$$\omega_k^{(n)}=\langle\varphi_n(r,\theta)|\hat{\xi_k^\gamma}(R_\infty,r,\theta)\rangle. \tag{25}$$

Thus, analogous to the Lanczos algorithm described above, a single sequence of Chebyshev iterations allows us to calculate *both* energies and product state distributions for different resonances.

III. CALCULATIONS

A. The Hamiltonian

The triatomic HO_2 Hamiltonian with total angular momentum $J=0$ is written in terms of Jacobi coordinates

$$\hat{H}=-\frac{\hbar^2}{2\mu_{\mathrm{H,O_2}}}\frac{1}{R}\frac{\partial^2}{\partial R^2}R-\frac{\hbar^2}{2\mu_{\mathrm{O_2}}}\frac{1}{r}\frac{\partial^2}{\partial r^2}r+\frac{\hbar^2}{2}\left(\frac{1}{\mu_{\mathrm{H,O_2}}R^2}+\frac{1}{\mu_{\mathrm{O_2}}r^2}\right)\hat{j}^2+V(R,r,\theta), \tag{26}$$

where R is the separation of H from the center of mass of O_2, r is the O–O separation, θ is the bend angle, and $\mu_{\mathrm{H,O_2}}$ and $\mu_{\mathrm{O_2}}$ are reduced masses. For current purposes, we utilize the HO_2 DMBE IV PES,[37] which has an equilibrium geometry of $R_e=2.466\,69\,a_0$, $r_e=2.514\,27\,a_0$, and $\theta_e=0.804\,81$ rad, and has a dissociation energy of 2.378 377 eV to the $H+O_2$ limit.

The Hamiltonian was then represented in a potential-optimized discrete variable representation[38] (PODVR). For the R coordinate, we used $N_R=120$ PODVR points, which were contracted from 350 evenly spaced primitive Sinc DVR points[39] spanning the range from 0.5 to $11.0\,a_0$ with the one-dimensional reference potential $V(R,r_e,\theta_e)$. Similarly, for the r coordinate, $N_r=50$ PODVR points were obtained from 150 primary DVR points spanning the range from $1.3\,a_0$ to $5.0\,a_0$ using the reference potential $V(R_e,r,\theta_e)$. For the θ variable, $N_\theta=43$ symmetry-adapted DVR functions, defined by 86 Gauss–Legendre quadrature points, were employed to take account of the odd O–O exchange parity. The resulting direct product basis set was further contracted by discarding those points whose potential energies were higher than the cutoff energy $V_{\mathrm{cutoff}}=2.0$ eV, resulting in the final basis size of 105 781.

For the LHFD calculations, the absorbing potential in the dissociation channel of $H+O_2$ takes the following form:

$$\hat{V}_{\mathrm{abs}}(R)=\frac{V_0}{\cosh^2[(R_{\max}-R)/\lambda]}, \tag{27}$$

where $R_{\max}=11.0\,a_0$, and V_0 and λ are two adjusting parameters. For our purposes we take $V_0=2.0$ eV and $\lambda=0.5\,a_0$. For the ACFFD method, we used the following damping function:

$$\hat{\gamma}(R)=e^{-\hat{V}_{sba}(R)}. \tag{28}$$

The rovibrational eigenfunctions of O_2 are direct products, written

$$\varphi_n=\frac{1}{r}|\nu\rangle|j\rangle. \tag{29}$$

Reuse of AIP Publishing content is subject to the terms: https://publishing.aip.org/authors/rights-and-permissions. Downloaded to IP: 130.102.82.69 On: Fri, 07 Oct 2016 05:32:49

The j-dependent radial vibrational components satisfy the radial Schrödinger equation

$$\left[-\frac{\hbar^2}{2\mu_{O_2}}\frac{d^2}{dr^2}+\frac{j(j+1)\hbar^2}{2\mu_{O_2}r^2}+V_{O_2}(r)\right]|\nu\rangle=\varepsilon_n|\nu\rangle. \quad (30)$$

For total angular momentum $J=0$, and for our choice of body-fixed frame, the Z axis is defined to be parallel to R such that O_2 and lies in XZ plane. Then

$$|j\rangle=\sqrt{\frac{(2j+1)}{2}}P_j(\cos\theta), \quad (31)$$

where P_j is a Legendre polynomial of degree n. We take a slice of HO_2 PES $V(R_\infty,r,\theta_e)$ as O_2 potential and use r PODVRs described above to solve Eq. (30) to get $|\nu\rangle$ and ε_n.

B. Resonance energies and widths

We have employed both the LHFD and ACFFD methods described in detail above to compute resonance energies and widths window by window in the energy range of 0.09 to 0.47 eV. In the LHFD approach, we set up a Lanczos subspace of order $M=40\,000$, and stored the two sets $\{a_k\}_1^M$ and $\{\beta_k\}_2^M$ for subsequent construction of the subspace matrices. In ACFFD, a sequence of 87 768 autocorrelation functions (for a propagation time of 275 592 a.u.) was needed to sufficiently converge the desired resonances, requiring $k_{\max}\cong 205\,000$. Eight energy windows of width 0.0475 eV have been used, each with 200 basis functions, to perform the FD calculations. Plotted in Fig. 1 are the calculated resonance energies and rates. Note that the rates are widths divided by $\hbar$, and therefore are true unimolecular decay rates only for narrow isolated resonances. Nevertheless, for simplicity, we will use rates independent of the energy regime, following the work of Schinke *et al.*[5] Besides, broader resonances cannot be extracted from the spectrum, simply because they are hidden in the background.

From Fig. 1 we see that resonance energies acquired via LHFC and ACFFD are in fairly sound agreement (i.e., 3 or 4 digits of relative accuracy). The resonance rates predicted by both methods agree within 20% of one another. To demonstrate the agreement more clearly we have shown an amplified part of the spectrum in Fig. 1(b). Analysis of the resonance widths shows that only at very low energies, these resonances are isolated. With increasing energy the resonances begin to overlap. The quantum widths (rates) show a large fluctuation, with the general tendency that the rates increase with energy. Just above threshold, the rates vary over three orders of magnitude, then the extent of fluctuation decreases with increasing energy. This fluctuating behavior has also been obtained by other theoretical calculations on HO_2 dissociation.[5,13,30] Although experimental data are still not available for this system, fluctuating resonance rates have been observed for several other dissociation systems including H_2CO, CH_3O, and NO_2.[40–42]

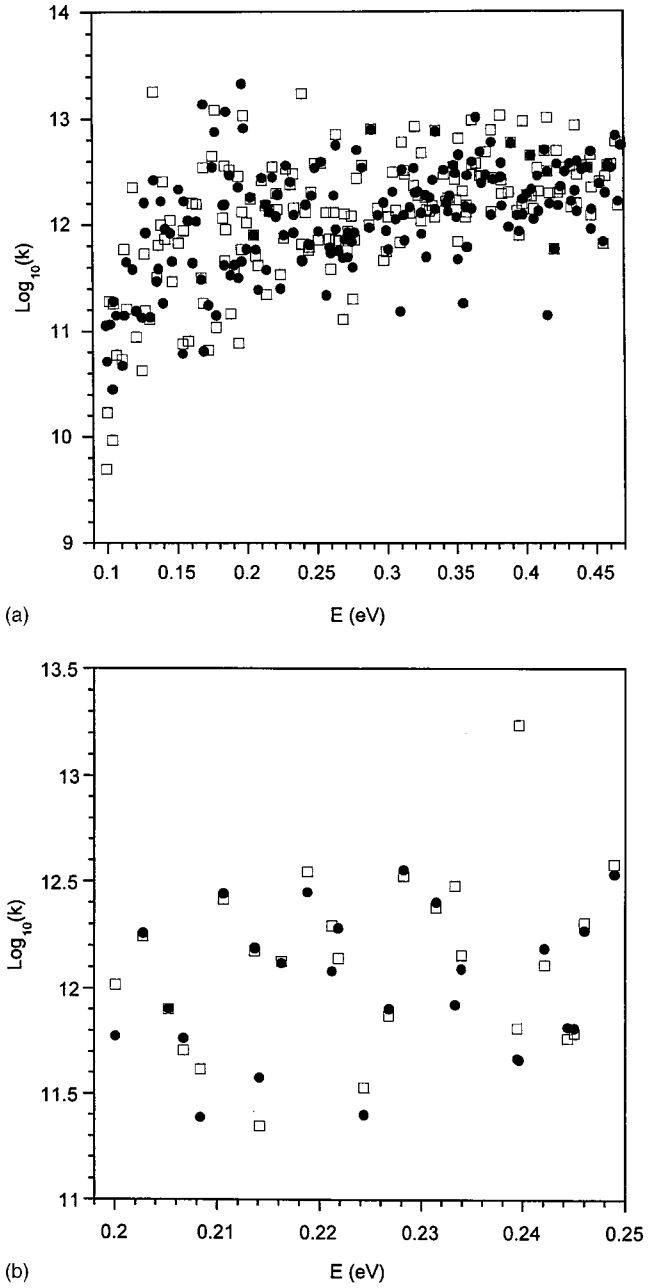

FIG. 1. (a) Plot of the logarithmic resonance rates, $\log_{10}(k)$, vs resonance energy in the energy range 0.09 to 0.47 eV. Circles represent the results from LHFD calculations and squares denote the results from ACFFD. The unit of decay rate is s^{-1}. (b) An amplified part of (a) in the energy range 0.2 to 0.25 eV.

C. Rotational state distributions

Evident from the forms of Eqs. (13) and (24), it proved a straightforward (and low-storage) exercise to calculate final rotational distributions for various energies and vibrational states of O_2. Figures 2(a)–2(d) show the O_2 rotational distributions for the ground vibrational state at different energies. Similarly, Figs. 3(a)–2(d) show the O_2 ($\nu=1$) rotational distributions at various energies. The general agreements among the two sets of calculations are satisfactory. For the $\nu=0$ rotational distributions, we can also compare with the results from the calculations of Schinke *et al.*;[5] for these resonances the general shapes and the nodal structures predicted by our calculations are quite similar to their results. We are unable to make such comparisons for the $\nu=1$ rotational distributions since these results appear here for the first time.

Reuse of AIP Publishing content is subject to the terms: https://publishing.aip.org/authors/rights-and-permissions. Downloaded to IP: 130.102.82.69 On: Fri, 07 Oct 2016 05:32:49

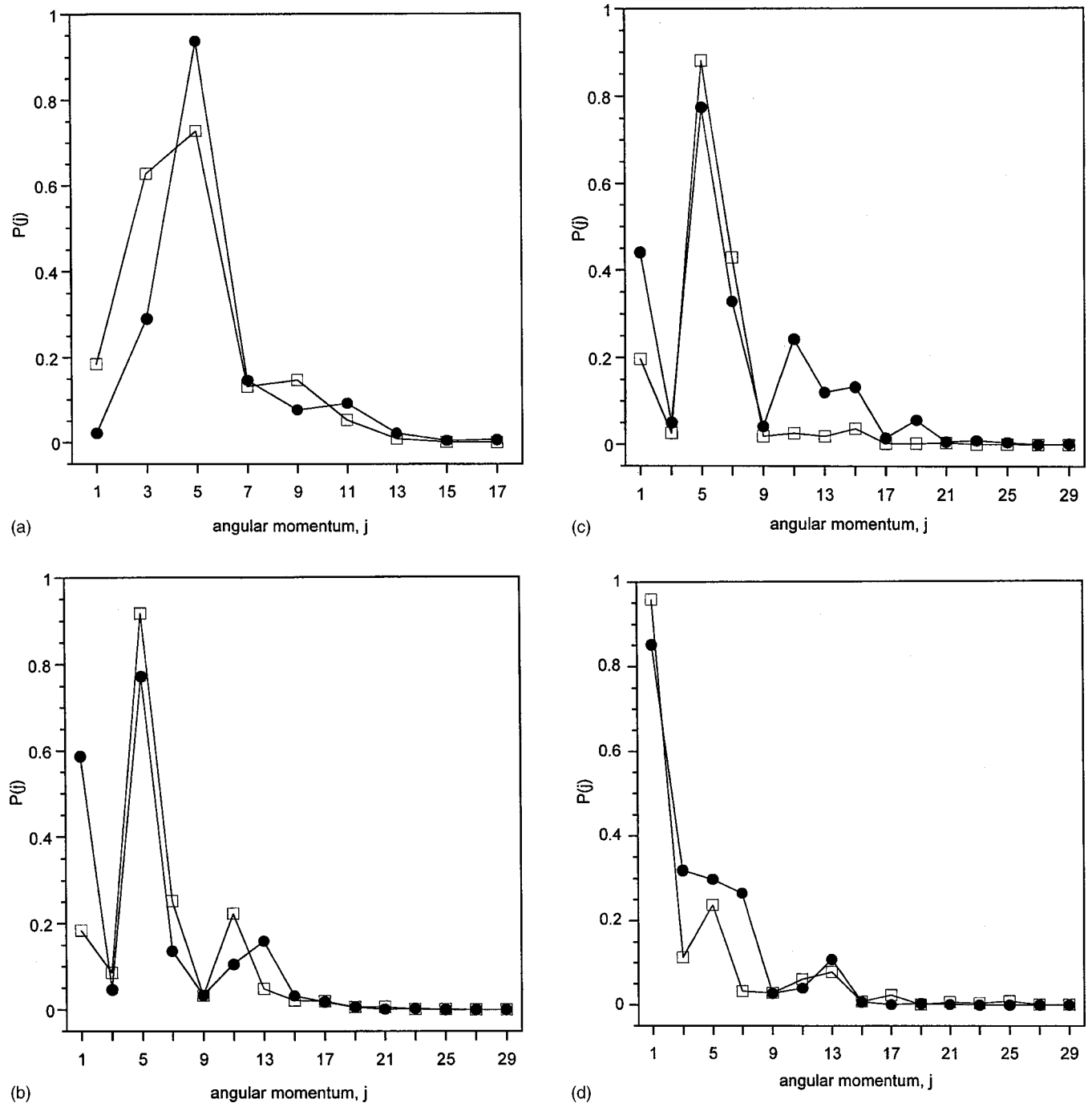

FIG. 2. (a) The O_2 ($\nu=0$) rotational distributions, $E=0.154$ eV. Symbols are the same as Fig. 1. All distributions are normalized. (b) Same as previous figure, except $E=0.252$ eV. (c) Same as previous figure, except $E=0.264$ eV. (d) Same as previous figure, except $E=0.362$ eV.

By inspecting Figs. 2 and 3, we can identify some general features and trends. First, the number of occupied rotational channels increases steadily with energy, which is simply the result of energy conservation. Second, the distributions show a very complicated oscillatory behavior, with the number of oscillations generally increasing with energy. Third, the fluctuations in the distributions seem to be random and unpredictable from resonance to resonance. (We have calculated *all* the rotational state distributions for $\nu=0$ and $\nu=1$ for the resonances lying between 0.09 to 0.47 eV. For brevity, only four for each vibrational state have been reported.)

The rotational state distributions of the fragments reflect the angular dependence of wave function at the translational state and the anisotropy of the PES in the exit channel. The rotational state distributions for the HO_2 dissociation are complicated mainly due to the translational–rotational coupling being weak but not negligible. The distributions cannot, therefore, be explained by a simple model such as the Franck–Condon mapping picture or the rotational reflection principle.[43] Similar irregular behavior has been observed experimentally for NO rotational state distributions associated with the unimolecular dissociation of NO_2.[44,45]

Reuse of AIP Publishing content is subject to the terms: https://publishing.aip.org/authors/rights-and-permissions. Downloaded to IP: 130.102.82.69 On: Fri, 07 Oct 2016 05:32:49

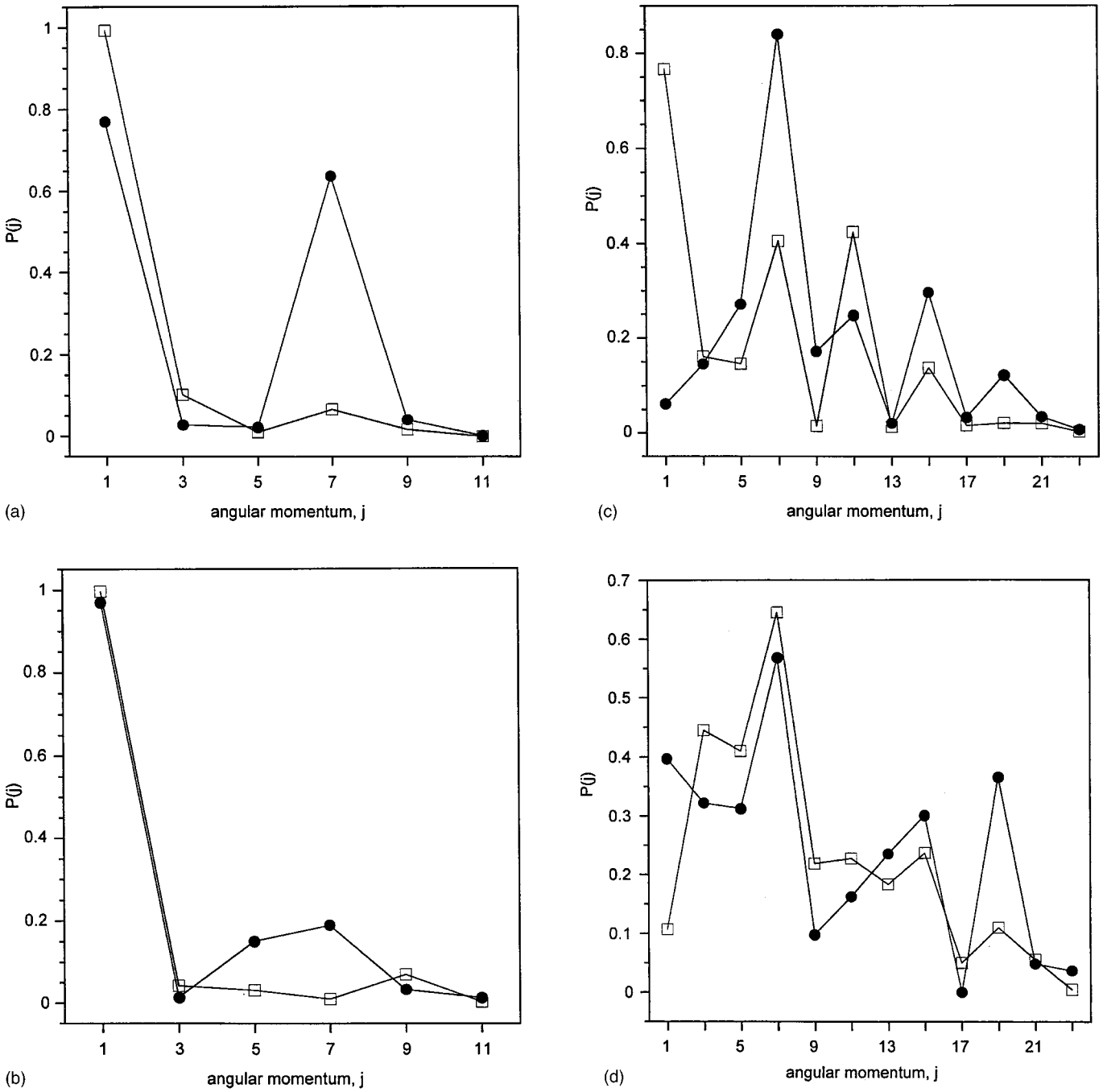

FIG. 3. (a) The O_2 ($\nu=1$) rotational distributions, $E=0.312$ eV. Symbols are the same as the previous figures. (b) Same as previous figure, except $E=0.321$ eV. (c) Same as previous figure, except $E=0.395$ eV. (d) Same as previous figure, except $E=0.421$ eV.

D. Vibrational product distributions

After obtaining the rotational distributions for $\nu=0$ and $\nu=1$, we can easily calculate the ratio of the number of O_2 molecules formed in the $\nu=1$ state to the number formed in the ground vibrational state, ρ_1/ρ_0. In Fig. 4, we see that the vibrational distributions fluctuate wildly from resonance to resonance, as can be expected from the rotational state distributions. The general trend is that the ratio increases with energy, approaching unity for the highest resonance energies. For all but several resonances, no population inversion was achieved in this energy range.

In our considered energy range, 0.294 eV (where the $\nu=1$ rotational manifold opens) up to 0.47 eV, most resonances are overlapping ones. When resonances overlap, interferences will occur. Thus, the wild fluctuations in Fig. 4 are a manifestation of prominent quantum interference effects between overlapping resonances. These kinds of fluctuating vibrational branching ratios have been observed in the dissociation of O_3.[46]

IV. CONCLUSION

In this paper we have reported quantum-mechanical calculations of the resonance states of HO_2 dissociation using a Lanczos subspace filter diagonalization method, and have

Reuse of AIP Publishing content is subject to the terms: https://publishing.aip.org/authors/rights-and-permissions. Downloaded to IP: 130.102.82.69 On: Fri, 07 Oct 2016 05:32:49

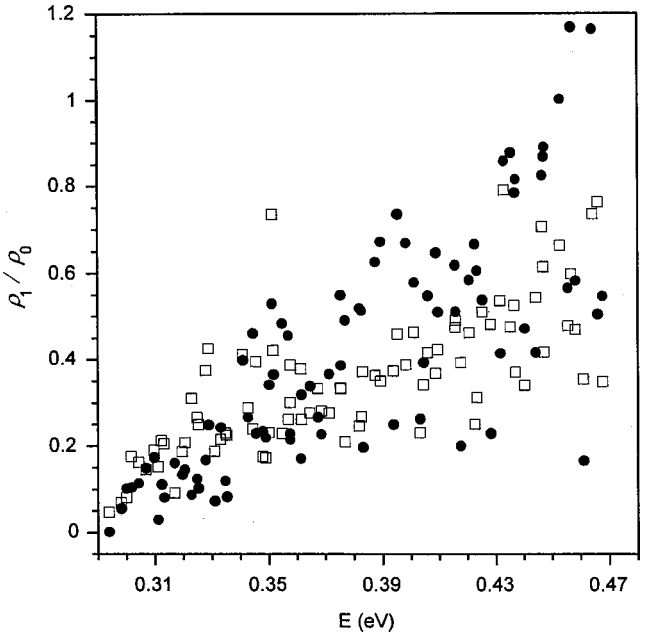

FIG. 4. The vibrational state distributions between $\nu=1$ and $\nu=0$. Other symbols are the same as the previous figures.

compared the results with an autocorrelation function-based filter diagonalization scheme. From a single set of Lanczos or Chebyshev iterations, selected resonances *and* PSDs can be efficiently obtained. The resonance energies from the two methods agree quite well, and resonance widths (rates) and PSDs are in sound agreement.

The unimolecular dissociation of HO_2 is dominated by resonances starting just above dissociation threshold. At low energies, these resonances are mainly isolated. With increasing energy, the resonances overlap, and the interferences among them lead to complicated dissociation dynamics. The resonance widths show strong fluctuations, and the extent of these fluctuations decreases with increasing energy. Rotational state distributions of O_2 show a very complicated oscillatory behavior, with the number of oscillations generally increasing with energy. The vibrational distributions between $\nu=1$ and $\nu=0$ also fluctuate wildly from resonance to resonance, and this ratio increases with energy, but population inversion is achieved only for several resonances. These results indicate there is an intricate coupling between the internal degrees of freedom in dissociation, and that the HO_2 dissociation is essentially irregular.

Although comprehensive experimental data for the HO_2 dissociation are still not available, we believe, in the near future, these fluctuations and oscillations will be observed and compared with the results from the above calculations and those to follow.

ACKNOWLEDGMENTS

The authors are grateful to the Australian Research Council for supporting this work (Large Grant No. A29937112). Dr. Anthony Rasmussen is acknowledged for assistance with the manuscript and Dr. Hua-Gen Yu for helpful discussions.

[1] R. Schinke, H.-M. Keller, H. Flothmann, M. Stumpf, C. Beck, D. H. Mordaunt, and A. J. Dobbyn, Adv. Chem. Phys. **101**, 745 (1997).
[2] S. A. Reid and H. Reisler, Annu. Rev. Phys. Chem. **47**, 495 (1996).
[3] T. Baer and W. L. Hase, *Unimolecular Reaction Dynamics: Theory and Experiments* (Oxford University Press, New York, 1996).
[4] S. C. Smith, in *Encyclopedia of Computational Chemistry*, edited by H. F. Schaefer (Wiley, New York, 1998).
[5] A. J. Dobbyn, M. Stumpf, H.-M. Keller, and R. Schinke, J. Chem. Phys. **104**, 8357 (1996).
[6] R. Q. Zhang, K. L. Han, R. S. Zhu, C. S. Lee, and S. T. Lee, Chem. Phys. Lett. **321**, 101 (2000).
[7] A. J. F. Siegert, Phys. Rev. **56**, 750 (1939).
[8] U. Peskin, H. Reisler, and W. H. Miller, J. Chem. Phys. **101**, 9672 (1994).
[9] H.-M. Keller and R. Schinke, J. Chem. Phys. **110**, 9887 (1999).
[10] D. Wang and J. M. Bowman, J. Chem. Phys. **100**, 1021 (1994).
[11] D. Neuhauser, J. Chem. Phys. **93**, 2611 (1990).
[12] M. R. Wall and D. Neuhauser, J. Chem. Phys. **102**, 8011 (1995).
[13] V. A. Mandelshtam, T. P. Grozdanov, and H. S. Taylor, J. Chem. Phys. **103**, 10074 (1995).
[14] V. A. Mandelshtam and H. S. Taylor, J. Chem. Phys. **107**, 6756 (1997).
[15] R. Chen and H. Guo, J. Chem. Phys. **111**, 464 (1999).
[16] M. Alacid, C. Leforestier, and N. Moiseyev, Chem. Phys. Lett. **305**, 258 (1999).
[17] H. G. Yu and S. C. Smith, Ber. Bunsenges. Phys. Chem. **101**, 400 (1997).
[18] H. G. Yu and S. C. Smith, J. Chem. Phys. **107**, 9985 (1997).
[19] H. G. Yu and S. C. Smith, Chem. Phys. Lett. **283**, 69 (1998).
[20] H.-G. Yu and S. C. Smith, J. Comput. Phys. **143**, 484 (1998).
[21] H. Zhang and S. C. Smith, Phys. Chem. Chem. Phys. **3**, 2282 (2001).
[22] M. Feit, J. A. Fleck, Jr., and A. Steiger, J. Comput. Phys. **47**, 412 (1982).
[23] M. Feit and J. A. Fleck, Jr., J. Chem. Phys. **78**, 301 (1983).
[24] V. A. Mandelshtam and H. S. Taylor, J. Chem. Phys. **103**, 2903 (1995).
[25] V. A. Mandelshtam and H. S. Taylor, J. Chem. Phys. **102**, 7390 (1995).
[26] B. Kendrick and R. T Pack, Chem. Phys. Lett. **235**, 291 (1995).
[27] B. Kendrick and R. T Pack, J. Chem. Phys. **104**, 7475 (1996).
[28] J. Dai and J. Z. H. Zhang, J. Phys. Chem. **100**, 6899 (1996).
[29] D. H. Zhang and J. Z. H. Zhang, J. Chem. Phys. **101**, 3671 (1994).
[30] A. J. Dobbyn, M. Stumpf, H.-M. Keller, W. L. Hase, and R. Schinke, J. Chem. Phys. **102**, 586 (1995).
[31] C. Lanczos, J. Res. Natl. Bur. Stand. **45**, 255 (1950).
[32] G. Moro and J. H. Freed, J. Chem. Phys. **74**, 3757 (1981).
[33] G.-J. Kroes and D. Neuhauser, J. Chem. Phys. **105**, 8690 (1996).
[34] M. Abramowitz and I. A. Stegun, *Handbook of Mathematical Functions* (NBS, U.S. GPO, Washington, DC, 1964).
[35] V. A. Mandelshtam and H. S. Taylor, J. Chem. Soc., Faraday Trans. **93**, 847 (1997).
[36] Y. Huang, W. Zhu, D. J. Kouri, and D. K. Hoffman, Chem. Phys. Lett. **206**, 96 (1993).
[37] M. R. Pastrana, L. A. M. Quintales, J. Brandao, and A. J. C. Varandas, J. Phys. Chem. **94**, 8073 (1990).
[38] J. Echave and D. Clary, Chem. Phys. Lett. **190**, 225 (1992).
[39] D. T. Colbert and W. H. Miller, J. Chem. Phys. **96**, 1982 (1992).
[40] A. Geers, J. Kappert, F. Temps, and J. W. Wiebrecht, J. Chem. Phys. **99**, 2271 (1993).
[41] W. H. Miller, R. Hernandez, C. B. Moore, and W. F. Polik, J. Chem. Phys. **93**, 5657 (1990).
[42] S. A. Reid and H. Reisler, J. Phys. Chem. **100**, 474 (1996).
[43] R. Schinke, *Photodissociation Dynamics* (Cambridge University Press, Cambridge, UK, 1993).
[44] U. Robra, H. Zacharias, and K. H. Welge, Z. Phys. D: At., Mol. Clusters **16**, 175 (1990).
[45] J. Miyawaki, K. Yamanouchi, and S. Tsuchiya, J. Chem. Phys. **99**, 254 (1993).
[46] M.-A. Thelen, T. Geju, J. A. Harrison, and J. R. Huber, J. Chem. Phys. **103**, 7946 (1995).

Reuse of AIP Publishing content is subject to the terms: https://publishing.aip.org/authors/rights-and-permissions. Downloaded to IP: 130.102.82.69 On: Fri, 07 Oct 2016 05:32:49